Original

Hieronymus, M.; Carpenter, J.R.:

Energy and Variance Budgets of a Diffusive Staircase with Implications for Heat Flux Scaling

In: Journal of Physical Oceanography (2016) AMS

DOI: 10.1175/JPO-D-15-0155.1

Energy and Variance Budgets of a Diffusive Staircase with Implications for Heat Flux Scaling

MAGNUS HIERONYMUS AND JEFFREY R. CARPENTER

Institute of Coastal Research, Helmholtz-Zentrum Geesthacht, Geesthacht, Germany

(Manuscript received 17 August 2015, in final form 1 May 2016)

ABSTRACT

The steady-state energy and thermal variance budgets form the basis for most current methods for evaluating turbulent fluxes of buoyancy, heat, and salinity. This study derives these budgets for a double-diffusive staircase and quantifies them using direct numerical simulations; 10 runs with different Rayleigh numbers are considered. The energy budget is found to be well approximated by a simple three-term balance, while the thermal variance budget consists of only two terms. The two budgets are also combined to give an expression for the ratio of the heat and salt fluxes. The heat flux scaling is also studied and found to agree well with earlier estimates based on laboratory experiments and numerical simulations at high Rayleigh numbers. At low Rayleigh numbers, however, the authors find large deviations from earlier scaling laws. Last, the scaling theory of Grossman and Lohse, which was developed for Rayleigh–Bénard convection and is based on the partitioning of the kinetic energy and tracer variance dissipation, is adapted to the diffusive regime of double-diffusive convection. The predicted heat flux scalings are compared to the results from the numerical simulations and earlier estimates.

1. Introduction

An interesting feature of the double-diffusive phenomena is its ability to create staircase-like structures in temperature and salinity, where well-mixed layers are separated by thin, high gradient interfaces (Radko 2013). Double-diffusive convection occurs in two different regimes: the diffusive and the finger regime. The focus in this article is on the diffusive regime, which occurs in waters where the temperature gradient is gravitationally unstable and the salinity gradient is stable. The finger regime on the other hand is commonplace in waters where the salinity gradient is stable and the temperature gradient is unstable. The density gradient is gravitationally stable in both regimes. Double-diffusive staircases in the diffusive regime are common in the polar oceans (Foster and Carmack 1976; Padman and Dillon 1989; Timmermans et al. 2008). In fact, the Arctic staircases have been suggested to be of great importance for the global climate since they are situated between cold surface waters and the warmer water of Atlantic origin, and there is enough heat trapped in the Atlantic Water to melt all Arctic sea ice within 4 yr if all the heat could be brought instantly to the surface (Turner 2010). Diffusive staircases are also important features in numerous lakes [see Wüest et al. (2012) and references therein] and fjords (Farmer and Freeland 1983; Pérez-Santos et al. 2014).

Much effort has been put into parameterizing the double-diffusive heat and salt fluxes because of their potential importance for the climate system on both a regional and global scale (Radko 2013). However, the very large parameter space in which these phenomena exist in nature makes it very difficult to find accurate parameterizations that apply globally. In this article, we will explore part of this parameter space by performing direct numerical simulations (DNS) of double diffusion at various values of the dimensionless thermal forcing, quantified by the Rayleigh number Ra. There are still only a small number of studies of diffusive convection that has used such a direct computational approach, and the only other study that we are aware of that has systematically probed the Ra range is Flanagan et al. (2013). There is, however, much motivation for such studies since the most commonly asked question in studies of diffusive convection is how the vertical fluxes of heat and salt depend on the problem parameters. We will explore this by looking at how the nondimensional

Corresponding author address: Magnus Hieronymus, Institute of Coastal Research, Helmholtz-Zentrum Geesthacht, Max-Planck-Strasse 1, 21502 Geesthacht, Germany.
E-mail: hieronymus.magnus@gmail.com

DOI: 10.1175/JPO-D-15-0155.1

heat flux, given by the Nusselt number Nu, depends on the Rayleigh number.

An often used assumption is that the heat flux in a diffusive staircase should be independent of the depths of the well-mixed layers as long as they are sufficiently deep (i.e., for sufficiently large Ra). This assumption leads to a functional dependence of the form $\mathrm{Nu} \propto \mathrm{Ra}^{1/3}$, which can also be expressed in terms of the heat flux F_T and its dependence on the top to bottom temperature difference ΔT, as $F_T \propto \Delta T^{4/3}$. This form is commonly referred to as the 4/3 law. The applicability of the 4/3 law has, however, been questioned, and revised exponents have been suggested by, for example, Kelley (1990), Kelley et al. (2003), Sommer et al. (2013), and Flanagan et al. (2013). The diffusive regime of double-diffusive convection has many similarities with the classical Rayleigh–Bénard convection problem for which several different regimes with different $\mathrm{Nu} \propto \mathrm{Ra}^b$ scaling laws have been found [see Ahlers et al. (2009) for a recent review]. Given the vast range of Ra in which double-diffusive staircases are found in nature, as well as the dependence of the fluxes on other variables (e.g., the Prandtl number, the diffusivity ratio, and the density ratio), it seems unlikely that a single power law that accurately parameterizes double-diffusive fluxes for the various different ocean and lake environments should exist. It is therefore important to understand the limitations of such heat flux parameterizations.

In this paper, we will make a careful examination of the physical basis for most current heat flux parameterizations, namely, the budgets of energy and tracer variance. These budgets form the basis of a number of methods used to indirectly measure and parameterize heat and salt fluxes. Based on the steady-state energy budget, there is the classical Osborn (1980) model, and from the thermal variance budget, we have the Osborn and Cox (1972) model. The application of both of these models to double diffusion is discussed in McDougall and Ruddick (1992). Moreover, these budgets form the basis of the so-called GL theory (Grossmann and Lohse 2000, 2001, 2002, 2004), which successfully predicts accurate flux laws for Rayleigh–Bénard convection. In this paper, we carefully derive approximate energy and variance budgets for a diffusive staircase that is found to agree extremely well with the results of our DNS. Furthermore, these approximate budgets are very similar to their counterpart for Rayleigh–Bénard convection used in the GL theory. We therefore believe that GL theory and the methodology behind it can be useful also for diffusive convection, and an extension of the theory for diffusive convection is presented.

Some attempts have been done at comparing double-diffusive fluxes derived from microstructure measurements, with those based on flux laws. Sommer et al. (2013), who took measurements in Lake Kivu on the border between the Democratic Republic of the Congo and Rwanda, and Guthrie et al. (2015), who took their measurements in the Amundsen Basin in the Arctic Ocean, are two examples. Both these studies support a downward revision of the commonly used Rayleigh number exponent of 1/3. However, the two studies support rather different revised exponents, 0.2 in the case of Sommer et al. (2013) and 0.29 in the case of Guthrie et al. (2015),[1] and there is a large scatter of points in both studies. The Rayleigh numbers are generally larger in the Amundsen Basin than in Lake Kivu with a mean value of 10^9 compared to 2.4×10^8 for the latter location, but there is a large spread within each staircase and Rayleigh numbers vary between about 10^5 and 10^{10} at both locations. We believe that one of the reasons for the large spread in the estimated exponents could be that a single exponent flux law is not generally enough to accurately describe diffusive convection throughout the world's oceans and lakes. For thermal convection, it is well known that the scaling exponents are functions of the Rayleigh number, and a key result in the GL theory is that these different regimes correspond to flow configurations where the kinetic energy and thermal variance dissipation are dominated by dissipation either in the boundary or the mixed layers. The results of our simulations, as well as the large spread of estimates in the literature, seem to suggest that such a division into regimes may be needed also for a flux law applicable to the global ocean. Application of the GL theory to diffusive convection is therefore a step toward finding a more general flux law than has previously existed for oceanic application.

The remainder of this manuscript is structured as follows: In section 2, we present the DNS model and the model setup and give a brief description of the flow. Section 3 contains a careful derivation of the energy budget and shows the resulting energy budgets from our DNS. In section 4, we present the tracer variance budgets from our DNS and discuss some theoretical results pertaining to those. Section 5, contains results for the heat flux scaling from our DNS and the application of GL theory to diffusive convection. The paper is concluded with a discussion and conclusions section.

2. Direct numerical simulations

a. *Model setup*

Our simulations are 2D, Boussinesq, and use a linear equation of state. 2D simulations of double diffusion are

[1] The exponent found by Guthrie et al. (2015) could also be as low as 0.25 depending on how one defines the layer thickness in the Rayleigh number definition.

much more computationally cost efficient than their 3D counterparts, and were found to capture the fluxes well for a density ratio $R_\rho \geq 3$ by Flanagan et al. (2013). We have also verified this by performing a 3D simulation that compares well to its 2D counterpart. The model setup is the same as that used by Sommer et al. (2014), where it was found to give fluxes in remarkable agreement with their observed values from Lake Kivu. The domain size is 0.66 m in the horizontal and 0.33 m in the vertical for the 2D runs, and the 3D run has a domain size of 0.33 m in both the horizontal and vertical directions. All simulations are initiated with horizontally uniform hyperbolic tangent profiles for T and S with an initial interface thickness of 0.03 m. Periodic boundary conditions are used on all boundaries, but ΔT and ΔS (the initial temperature and salinity differences between the top and the bottom of the domain) are added or subtracted to water parcels crossing the vertical boundary so that a steady state can be upheld.

The simulations are done using the DNS code of Winters et al. (2004) and are governed by the following nondimensional numbers:

$$\mathrm{Pr} \equiv \frac{\nu}{\kappa_T} = 6.25, \quad \tau \equiv \frac{\kappa_S}{\kappa_T} = 0.01,$$
$$R_\rho \equiv -\frac{\rho_T \Delta T}{\rho_S \Delta S} = 5 \quad \text{and} \quad \mathrm{Ra} \equiv \frac{g\rho_T \Delta T H^3}{\nu \kappa_T \rho_0}, \qquad (1)$$

where Pr is the Prandtl number, ν is the kinematic viscosity, $\kappa_{T(S)}$ is the thermal (haline) diffusivity, τ is the diffusivity ratio, $\rho_{T(S)}$ is the partial derivative of density with respect to temperature (salinity; these are constants since we use a linear equation of state), R_ρ is the density ratio, g is the acceleration due to gravity, $\Delta T(S)$ is the top to bottom temperature (salinity) difference, H is the height of the domain, and ρ_0 is a constant reference density.

The grid resolution is chosen so that $\Delta x/L_B < 1$, where $L_B = (\nu\kappa_S^2\varepsilon_u^{-1})^{1/4}$ is the Batchelor scale for salinity, and ε_u is the dissipation of kinetic energy. Carpenter et al. (2012) found $\Delta x/L_B = 2$ to be somewhat inadequate to do accurate energy diagnostics, and we have therefore opted for a higher resolution. In total we have done 10 runs with different Ra by varying ΔT, while keeping the other nondimensional parameters constant at values [given in (1)] typical to the double-diffusive staircase in Lake Kivu. These values are also quite close to the representative Arctic values used by Flanagan et al. (2013; $R_\rho = 4$, $\tau = 0.005$, and $\mathrm{Pr} = 13$).

b. Flow description

In this section, we provide a basic description of the flow field in our simulations. Snapshots of the density field and its contributions from salinity and temperature from our run with $\mathrm{Ra} = 3.3 \times 10^6$ are shown in Figs. 1a–c. Figure 1a shows the density, Fig. 1b shows the salinity field contribution to the density, and Fig. 1c shows the temperature field's contribution to the density. The density panel is, as expected when $R_\rho = 5$, mostly reflecting the salinity field. It is also evident from inspecting the temperature and salinity fields that the lower diffusivity for salinity leads to much finer-scale features in this field.

The horizontally averaged horizontal velocity $\langle u \rangle_x$ from our run with $\mathrm{Ra} = 3.3 \times 10^6$ is shown in Fig. 2. Henceforth, we shall take $\langle\,\rangle_x$ to mean an average over the horizontal coordinate x, $\langle\,\rangle_{xy}$ is an average over a horizontal plane, and $\langle\,\rangle_{xyz}$ is a volume average. With periodic boundary conditions it is easy to show that $\int_z \langle u \rangle_x \, dz = C$, where C is some constant. Our runs are initiated with zero net horizontal advection (i.e., $C = 0$), and so they remain for the duration of the runs. A consequence of the zero net advection is that we tend to get opposing horizontal currents in the mixed layer above and below the interface. These currents represent a large-scale circulation cell in the mixed layer that is observed to change sign regularly. It can also be seen that the horizontal advection at the level of the interface, however, is mostly weak.

Another illustrative simplified picture of the flow can be obtained by projecting the flow into density depth space. Nycander et al. (2007) introduced a streamfunction in density depth coordinates and showed that it has several qualities that make it suitable for energetics studies. The density depth streamfunction Ψ is defined through

$$\Psi(\rho^*, z) = \frac{1}{t_2 - t_1} \int_{t_1}^{t_2} \int_{A(\rho^*, z, t)} w \, dA \, dt, \qquad (2)$$

where $\rho^* = 2(\rho - \rho_0)/\Delta\rho$ is a nondimensional density, and $A(\rho^*, z, t)$ is the area at depth z, where the density is less than ρ (in the 2D case this area is, in fact, a line). The quantity $\Psi(l, m)$ is thus the upward vertical volume transport of water lighter than l at depth m. This sign convention is the opposite of that used by Nycander et al. (2007) and makes a thermally direct cell (a cell where dense water sinks and lighter water rises) have a positive sign. Figure 3a shows the streamfunction, which in our case has a very simple form. There is just one circulation cell, which is thermally direct and occupies the mixed layers on both sides of the interface. The streamfunction amplitude in the interface is almost zero, which signifies that the interfacial advection is weak. The streamfunctions are qualitatively similar for all runs, but the amplitude increases with increased Ra, and the interface thickness decreases with increased Ra.

Water mass transformation can be thought of as a circulation in tracer space (see, e.g., Hieronymus et al. 2014) and is therefore often visualized using streamfunctions

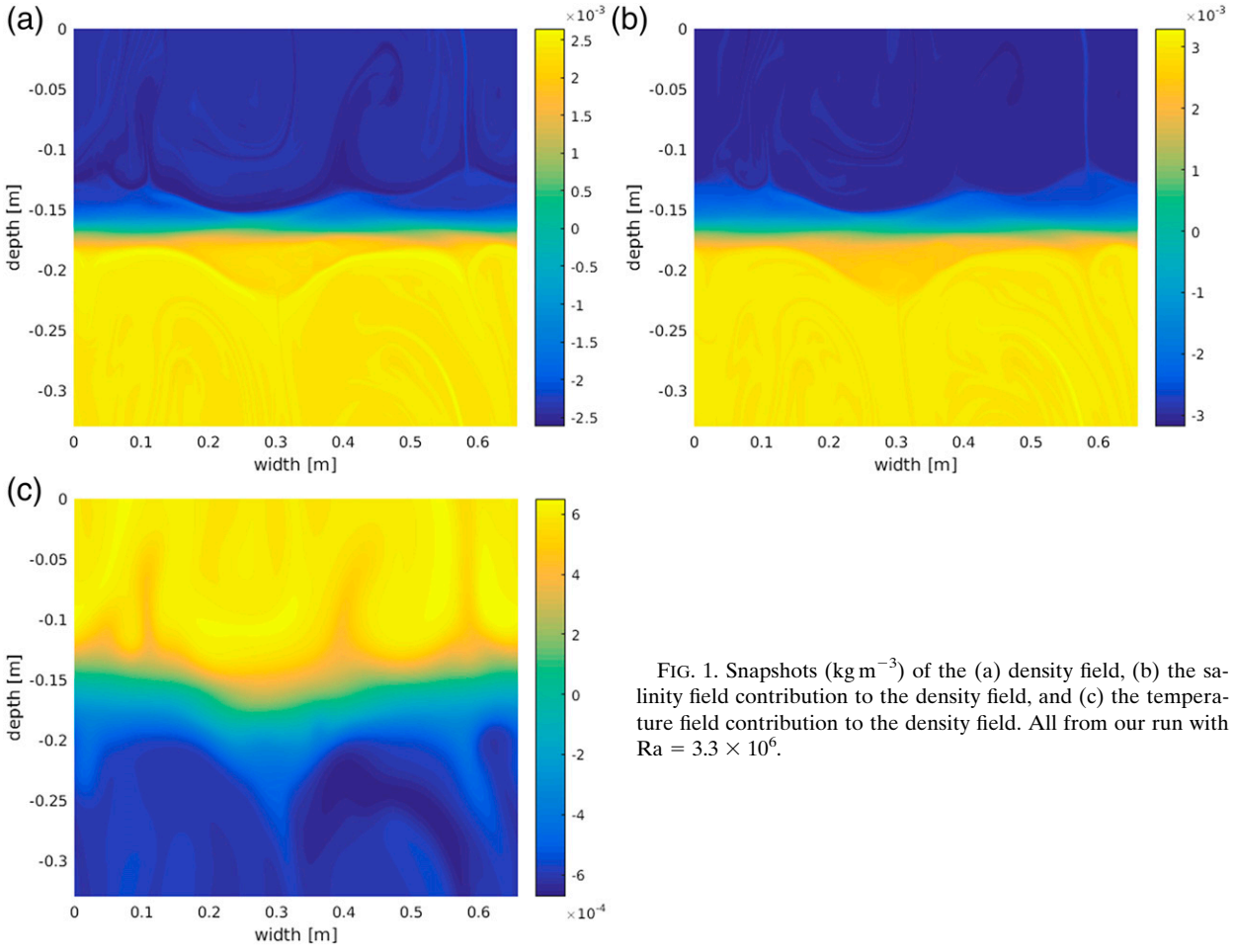

FIG. 1. Snapshots (kg m^{-3}) of the (a) density field, (b) the salinity field contribution to the density field, and (c) the temperature field contribution to the density field. All from our run with Ra $= 3.3 \times 10^6$.

where at least one coordinate is a tracer. In this case, we use density as a streamfunction coordinate, and the circulation in density space is analogous to a water mass transformation. The fact that there are very small density changes along the streamlines in the mixed layer therefore implies that the bulk of the transformation is achieved within or in close proximity to the interface. The strong circulation in the mixed layer plumes thus occur in a very narrow density band. This is even more apparent if we look at $\partial\Psi/\partial\rho$, shown in Fig. 3b. Since, as we stated before, $\Psi(l, m)$ gives the volume transport of water lighter than l at depth m, the vertical volume flux of water in a small density range at a given depth is given by $(\partial\Psi/\partial\rho)\Delta\rho$. This figure clearly shows how light water rises and dense water

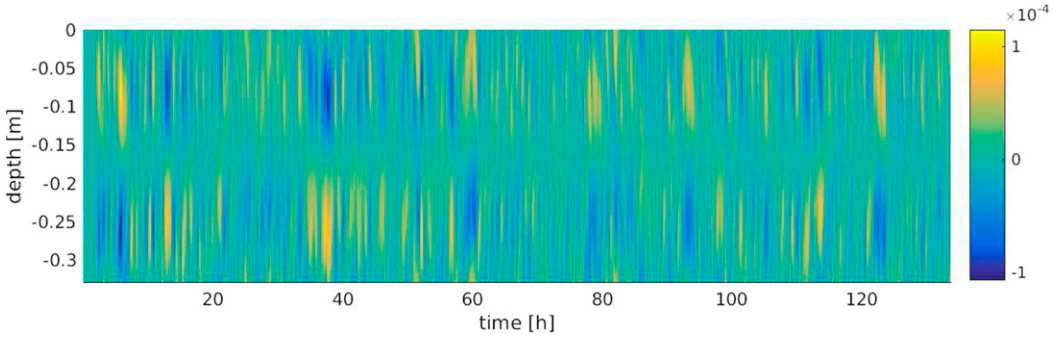

FIG. 2. Horizontally averaged horizontal velocity (m s^{-1}) as a function of t and z from our run with Ra $= 3.3 \times 10^6$.

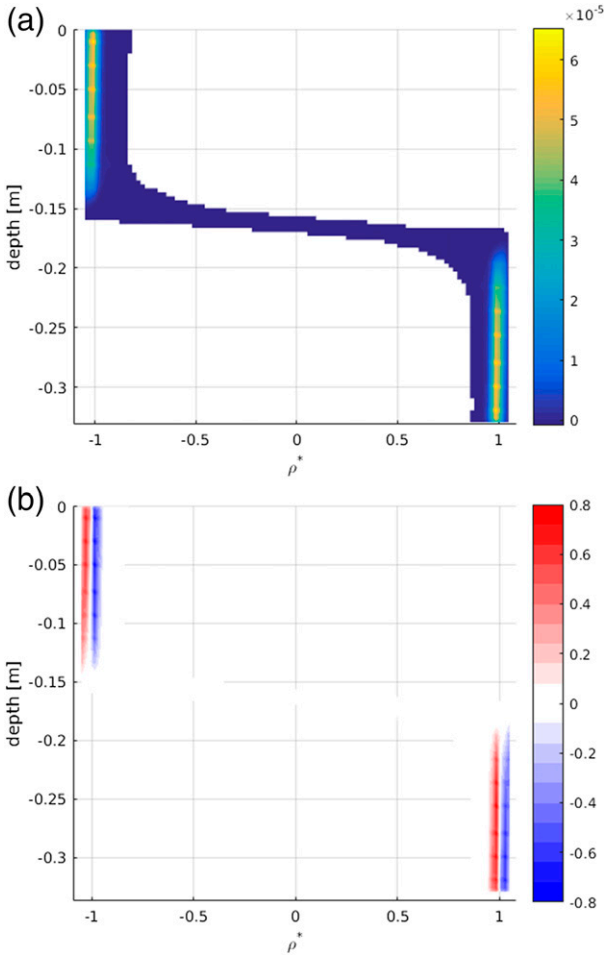

FIG. 3. (a) The streamfunction ($m^2\,s^{-1}$) in density depth coordinates. (b) $\partial\Psi/\partial\rho$ [$m^5\,(kg\,s)^{-1}$]. Both are based on the velocity field of the last 17 h from our run with Ra = 3.3×10^6.

sinks in the red and blue circulation branches, respectively. We should note, however, that Ψ is the result of a long time average (17 h in this case) and that individual parcel trajectories are not confined to follow the streamlines.

The double integral of Ψ over ρ and z multiplied by g gives the conversion between kinetic and potential energy. Nycander et al. (2007) used that result to calculate the contributions from different circulation cells in an ocean-only general circulation model. Our flow is more simple and consists of only one cell that occupies the mixed layer and converts potential energy into kinetic.

3. The energy budget

Here, we consider the energetics of a double-diffusive staircase using the Boussinesq approximation with a linear equation of state. The equations are as follows:

$$\rho_0 \frac{D\mathbf{u}}{Dt} = -\nabla p - \hat{\mathbf{z}} g\rho' + \mu\nabla^2\mathbf{u}, \tag{3}$$

$$\nabla\cdot\mathbf{u} = 0, \tag{4}$$

$$\rho' = \rho_T T + \rho_S S, \tag{5}$$

$$\frac{DT}{Dt} = \kappa_T \nabla^2 T, \tag{6}$$

$$\frac{DS}{Dt} = \kappa_S \nabla^2 S, \quad \text{and} \tag{7}$$

$$\frac{D}{Dt} = \frac{\partial}{\partial t} + \mathbf{u}\cdot\nabla, \tag{8}$$

where $\mathbf{u}$ is the velocity vector, p is pressure, ρ' is the deviation from the constant reference density ρ_0, $\hat{\mathbf{z}}$ is the unit vector in the vertical direction, and μ is the dynamic viscosity.

To get an equation for the kinetic energy we take the scalar product of (3) and $\mathbf{u}$ and use (4), yielding

$$\frac{D}{Dt}\left(\rho_0\frac{|u|^2}{2}\right) = -\nabla\cdot(\mathbf{u}p) - wg\rho' + \mu\nabla\cdot(u_i\nabla u_i) - \mu\nabla u_i\cdot\nabla u_i, \tag{9}$$

where u_i represents the three velocity components, and summation over repeated indices is understood. The last two terms are derived using the identity $\mathbf{u}\cdot\nabla\mathbf{u} = \nabla\cdot(u_i\nabla u_i) - \nabla u_i\cdot\nabla u_i$. To get an energy budget, we integrate (9) over a mixed layer in a diffusive staircase bounded at $z = 0$ and $z = -H$ by diffusive interfaces and with periodic boundaries in the horizontal; we call this volume V. Using Gauss's divergence theorem and Reynold's transport theorem the kinetic energy budget may be written as

$$\frac{d}{dt}\int_V \rho_0\frac{|u|^2}{2}dV = -\int_{\partial V}\rho_0\frac{|u|^2}{2}\mathbf{u}_{\text{out}}\cdot\hat{\mathbf{n}}\,dA - \int_{\partial V} p\mathbf{u}\cdot\hat{\mathbf{n}}\,dA - \int_V \rho' gw\,dV + \mu\int_{\partial V} u_i\nabla u_i\cdot\hat{\mathbf{n}}\,dA - \mu\int_V \nabla u_i\cdot\nabla u_i\,dV, \tag{10}$$

where $\mathbf{u}_b$ is the velocity of the boundary, $\hat{\mathbf{n}}$ is an outward unit vector normal to ∂V, and $\mathbf{u}_{\text{out}} = \mathbf{u} - \mathbf{u}_b$ is the velocity through the boundary. The first term on the right-hand side is the advective flux of kinetic energy, the second has the appearance of a boundary flux of pressure, the third is the buoyancy flux (or the conversion between kinetic

and potential energy), the fourth is due to work by viscous torques on the boundary, and the fifth is the dissipation ε_u of kinetic energy.

To derive the potential energy budget, we take the material derivative of (5) multiplied by gz and use (6) and (7), which gives

$$\frac{\partial gz\rho'}{\partial t} + \mathbf{u}\cdot\nabla(gz\rho') = gz(\rho_T\kappa_T\nabla^2 T + \rho_S\kappa_S\nabla^2 S) + wg\rho'. \tag{11}$$

Again, we integrate using the divergence theorem and Reynold's transport theorem to obtain

$$\frac{d}{dt}\int_V gz\rho'\,dV = -\int_{\partial V} gz\rho'\mathbf{u}_{\text{out}}\cdot\hat{\mathbf{n}}\,dA + \int_V g\nabla\cdot(z\rho_T\kappa_T\nabla T + z\rho_S\kappa_S\nabla S)\,dV - \int_V g\left(\rho_T\kappa_T\frac{\partial T}{\partial z} + \rho_S\kappa_S\frac{\partial S}{\partial z}\right)dV + \int_V wg\rho'\,dV. \tag{12}$$

As before, we integrate between $z = -H$ and $z = 0$ and use the horizontal periodicity. Equation (12) may then be written as

$$\frac{d}{dt}\int_V gz\rho'\,dV \approx \int_{\partial V_b} gH\rho'\mathbf{u}_{\text{out}}\cdot\hat{\mathbf{n}}\,dA + \int_{\partial V_b} gH(\rho_T\kappa_T\nabla T + \rho_S\kappa_S\nabla S)\cdot\hat{\mathbf{n}}\,dA - Ag(\rho_T\kappa_T\Delta T + \rho_S\kappa_S\Delta S) + \int_V wg\rho'\,dV, \tag{13}$$

where ∂V_b signifies that the integral is taken over the bottom interface, $\Delta T = T(0) - T(-H)$, $\Delta S = S(0) - S(-H)$, and A is the horizontal area of the domain. To arrive at (13) we have used the approximation that the interfaces are fixed at their respective vertical coordinates. This approximation is closely tied to another approximation we shall use, namely, that the interfacial advection is weak. These assumptions have proven to hold for diffusive convection when the density ratio $R_\rho = -\rho_S\Delta S/\rho_T\Delta T$ is larger than about 3 (Carpenter et al. 2012; Sommer et al. 2014; Carpenter and Timmermans 2014). The fact that the interfacial advection is weak is also evident from our streamfunction, plotted in Fig. 3. This means that the advective boundary terms can be neglected. Using this, and also assuming a steady state, the kinetic energy balance is given by

$$\int_V wg\rho'\,dV \approx -\mu\int_V \nabla u_i\cdot\nabla u_i\,dV, \tag{14}$$

that is, we have a balance between the buoyancy flux and the dissipation. Note that this means that the mixing efficiency (i.e., the ratio of the buoyancy flux to the dissipation) of double diffusion is approximately 1 and thus very different from the value of 0.2 that is often used in oceanography. Applying the same approximations to the potential energy budget yields

$$\int_{\partial V_b} gH(\rho_T\kappa_T\nabla T + \rho_S\kappa_S\nabla S)\cdot\hat{\mathbf{n}}\,dA \approx Ag(\rho_T\kappa_T\Delta T + \rho_S\kappa_S\Delta S) - \int_V wg\rho'\,dV, \tag{15}$$

which can also be written using (14) as

$$\int_{\partial V_b} gH(\rho_T\kappa_T\nabla T + \rho_S\kappa_S\nabla S)\cdot\hat{\mathbf{n}}\,dA \approx Ag(\rho_T\kappa_T\Delta T + \rho_S\kappa_S\Delta S) + \mu\int_V \nabla u_i\cdot\nabla u_i\,dV. \tag{16}$$

Now we define

$$\rho_0 AH\langle F_b\rangle_{xy} \equiv \int_{\partial V_b} gH(\rho_T\kappa_T\nabla T + \rho_S\kappa_S\nabla S)\cdot\hat{\mathbf{n}}\,dA, \tag{17}$$

$$\rho_0 AH\langle F_b^{\text{cond}}\rangle_{xyz} \equiv Ag(\rho_T\kappa_T\Delta T + \rho_S\kappa_S\Delta S), \quad \text{and} \tag{18}$$

$$\rho_0 AH\langle\varepsilon_u\rangle_{xyz} \equiv \mu\int_V \nabla u_i\cdot\nabla u_i\,dV, \tag{19}$$

where $\langle F_b\rangle_{xy}$ is the average interfacial buoyancy flux, $\langle F_b^{\text{cond}}\rangle_{xyz}$ is the volume-averaged diffusive buoyancy flux, and $\langle\varepsilon_u\rangle_{xyz}$ is the volume-averaged dissipation of kinetic energy. Equation (16) can then be written as

$$\text{Nu}_b \approx 1 + \frac{\langle\varepsilon_u\rangle_{xyz}}{\langle F_b^{\text{cond}}\rangle_{xyz}}, \tag{20}$$

where $\text{Nu}_b \equiv \langle F_b\rangle_{xy}\big/\langle F_b^{\text{cond}}\rangle_{xyz}$ is the Nusselt number for the buoyancy flux, that is, the ratio of the buoyancy flux through the interface to the purely conductive value. Using (14), (20) can also be written as

$$\text{Nu}_b \approx 1 + \text{Nu}_b^{\text{adv}}, \tag{21}$$

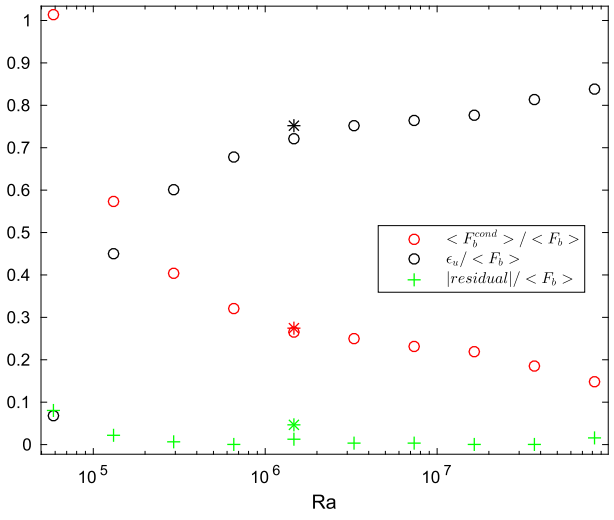

FIG. 4. The energy budget nondimensionalized through division by F_b. Asterisks show the results from the 3D run.

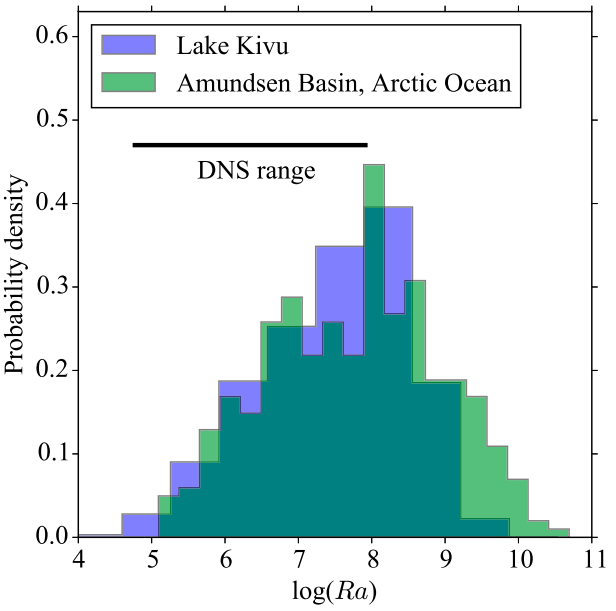

FIG. 5. Ra distributions from the diffusive staircases in Lake Kivu and the Amundsen Basin in the Arctic Ocean. The Kivu data come from Sommer et al. (2013), and the Arctic data come from Guthrie et al. (2015). The black line signifies the Ra range in our DNS.

where $\mathrm{Nu}_b^{\mathrm{adv}} \equiv \langle \rho' w g / \rho_0 \rangle_{xyz} \Big/ \langle F_b^{\mathrm{cond}} \rangle_{xyz}$ is a Nusselt number based only on the advective fluxes. The physical meaning of (21) is plainly that Nu_b is the sum of the purely conductive value of 1 and the contribution from advection. The energy budgets of the Boussinesq equations are altered when a more realistic nonlinear equation of state is used (Nycander 2011; Hieronymus and Nycander 2015). A discussion of these issues and a derivation of the equivalent of (20) for a nonlinear equation of state are presented in appendix A.

Equation (20) is a double-diffusive analog to the model developed by Osborn (1980) for the energy budget of shear-driven turbulence. It should also be noted that (14) is the most straightforward extension of Osborn's model to double diffusion. It is, however, as can be seen from (21), not very accurate in determining staircase fluxes unless $\mathrm{Nu}_b \gg 1$, so (20) is to be preferred. The important point here is that the interfacial buoyancy flux going through a staircase is different from the average advective buoyancy flux in the staircase, which is also often refereed to simply as the buoyancy flux. This difference stems from the fact that tracer transport is due to a mixture of advection and diffusion.

Figure 4 shows the energy budgets given by (16) from our different runs. The terms have been normalized through division by the largest term in the budgets $\langle F_b \rangle_{xy}$ so that they would sum to 1 if the approximate budget was perfect. The heat (salinity) flux is calculated by finding the temperature (salinity) gradient at the zero isotherm by linear interpolation, multiplying it by κ_T (κ_S), and then integrating along the isotherm [the same method is used by Carpenter and Timmermans (2014) and Sommer et al. (2014)]. For the range of Rayleigh numbers in our simulations, it is clear that (16), indeed, gives a very good approximation of the total energy budget in the 2D runs. The residual contains all contributions due to interfacial advection, temporal variability, and the fact that our domain is not entirely well defined[2] and is never greater than a couple of percent of $\langle F_b \rangle_{xy}$. In the 3D run, denoted here by an asterisk, we see a larger residual. This discrepancy between the 2D and 3D case is due to differences in the salt flux. The dissipation, in fact, agrees to within 1% between the two runs. The salt flux is more time variable than the heat flux, so a longer duration 3D run is likely to diminish this discrepancy.

The energy budget of Fig. 4 shows that $\langle F_b^{\mathrm{cond}} \rangle_{xyz}$ is significant in comparison to $\langle F_b \rangle_{xy}$ throughout the range of Ra in this study. Figure 5 shows how the Ra range in our simulations compare to staircases found in Lake Kivu and the Amundsen Basin in the Arctic Ocean. It is clear that there is a large overlap between our Ra range and that from these two locations. It is therefore important to consider the three-term energy balance derived here, that is, the Osborn model for diffusive convection [(20)], instead of the most straightforward extension of Osborn's model to double diffusion, namely, (14) when evaluating fluxes through staircases in oceans and lakes.

[2] The terms F_T and F_S are calculated at the zero isotherm and isohaline, respectively; however, those surfaces are not constantly collocated.

Another consequence of the steady-state energy balance is that the Batchelor scale for salinity $L_B = (\nu\kappa_S^2\varepsilon_u^{-1})^{1/4}$, which is the most critical scale that must be sufficiently resolved in double-diffusive DNS, is given by

$$L_B = \left(\frac{\nu\kappa_S^2}{\langle F_b\rangle_{xy} - \langle F_b^{\text{cond}}\rangle_{xyz}}\right)^{1/4}. \tag{22}$$

This form has the advantage over the conventional expression in that it contains $\langle F_b\rangle_{xy}$ rather than $\langle\varepsilon_u\rangle_{xyz}$, and one can therefore estimate L_B beforehand using a flux law.

Flanagan et al. (2013) use a slightly different scale than L_B to characterize the scale of salt dissipation, given by

$$L_S = \left(\frac{\nu\kappa_S^2}{\langle F_b^{\text{cond}_T}\rangle_{xyz}}\right)^{1/4}, \tag{23}$$

where $\langle F_b^{\text{cond}_T}\rangle_{xyz}$ is the part of $\langle F_b^{\text{cond}}\rangle_{xyz}$ that is due to temperature. The effect of temperature on $\langle F_b^{\text{cond}}\rangle_{xyz}$ is much larger than that due to salinity in the oceanographically relevant parameter range. Using this we can approximate the ratio of the scales as

$$\frac{L_S}{L_B} \approx (\text{Nu}_b - 1)^{1/4}. \tag{24}$$

The Nusselt numbers in our runs are too small [the ratio (24) is about 1.6] to make the two scales diverge significantly, and it is therefore impossible to make any claims about their respective relevance for salinity variance dissipation. It is nonetheless interesting to see that their ratio tends to infinity as Nu goes to infinity. This means that if it is truly enough to resolve L_S then simulating high Ra environments is somewhat less numerically demanding then one might expect from using L_B as the relevant scale. However, DNS studies of shear flows suggest that the grid spacing must, in fact, be comparable to the Kolmogorov scale, or the Batchelor scale when $\text{Pr} > 1$, for the flows to be well resolved (Smyth and Moum 2000; Moin and Mahesh 1998).

4. Thermal and haline variance budgets

Two models that are similar to the Osborn model for diffusive convection [(20)] can be constructed using the steady-state and zero interfacial advection assumptions to develop the budgets of thermal and haline variance. A model for the thermal case can be derived by multiplying (6) by T and integrating over the whole domain using the same assumptions that were used in deriving (20), which gives

$$\langle F_T\rangle_{xy} \approx -\frac{\kappa_T H}{\Delta T}\langle|\nabla T|^2\rangle_{xyz}, \tag{25}$$

where $\langle F_T\rangle_{xy}$ is the average interfacial temperature flux, and $\kappa_T\langle|\nabla T|\rangle_{xyz}^2 \equiv \varepsilon_T$ is the average dissipation of thermal variance. The haline case is completely analogous. Equation (25) is an integrated form of the famous Osborn and Cox (1972) relation, but in this case $\langle F_T\rangle_{xy}$ is diffusive rather than advective, as it is in the Osborn and Cox (1972) relation. Equation (25) can also be expressed in terms of the Nusselt number as

$$\text{Nu} \approx \frac{\langle|\nabla T|^2\rangle_{xyz}}{\left(\frac{\Delta T}{H}\right)^2}. \tag{26}$$

Equations (20) and (26) can also be combined to give an estimate for the flux ratio $R_f = -\rho_S F_S/\rho_T F_T$, according to

$$R_f = 1 - \frac{\left(\frac{\Delta T}{H}\right)^2}{\langle|\nabla T|^2\rangle}(1 - \tau R_\rho) + \frac{\frac{\Delta T}{H}}{b_T}\frac{\langle\varepsilon_u\rangle_{xyz}}{\langle\varepsilon_T\rangle_{xyz}}, \tag{27}$$

where $b_T = -g\rho_T/\rho_0$ is the partial derivative of buoyancy with respect to temperature. The flux ratio is thus dependent on two interesting ratios: the first is the ratio of the background temperature gradient to the thermal variance, which is equal to 1/Nu [see (26)], and the second is the ratio of the dissipation of kinetic energy to that of thermal variance.

Figure 6 shows how well the approximation of (25) captures the heat fluxes in our simulation with $\text{Ra} = 3.3 \times 10^6$ (the results are similar for all runs). It is interesting that this method works well throughout the duration of the run. This shows that the contributions to the variance budgets from interfacial advection and temporal variability are much smaller than the two terms in (25) long before we would classify the run as steady state.

5. Heat flux scaling

a. Results from DNS

We have seen in the preceding sections how the Nusselt number is linked to the budgets of energy and tracer variance. In this section, we shall go on to look at how Nu scales with Ra in our DNS and formulate the GL theory based on the partitioning of ε_T and ε_ν in the domain. Figure 7 shows a log–log plot of Nu(Ra) and demonstrates that a single power law is not adequate to describe the functional dependence of Nu on Ra in the whole parameter range of interest. However, piecewise

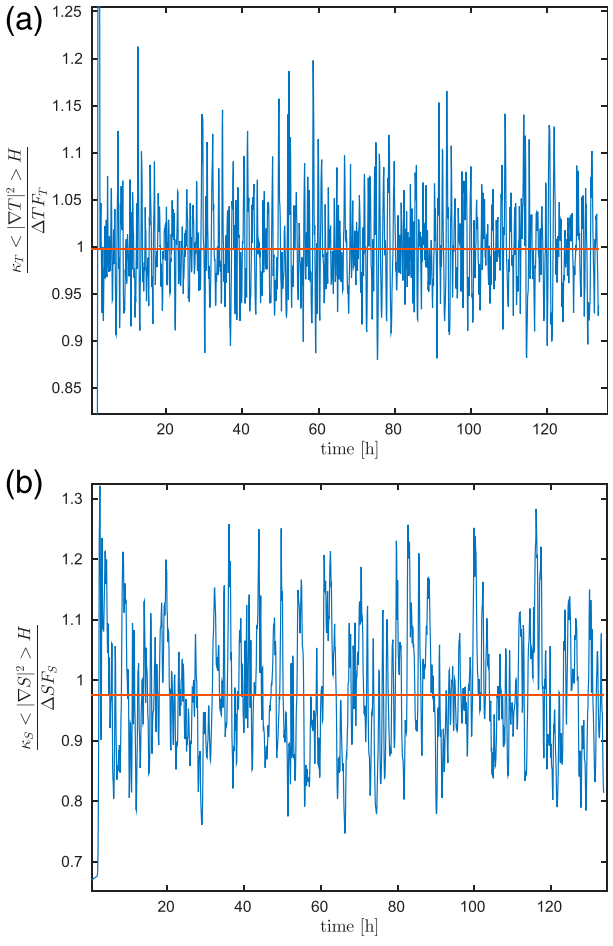

FIG. 6. The right-hand side of (25) divided by the left-hand side from our run with Ra = 3.3 × 10^6 for (a) temperature and (b) salinity. The brown lines show the mean value of the curves.

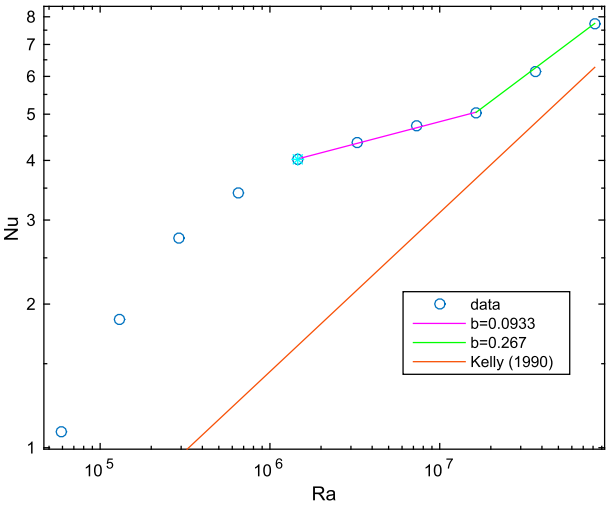

FIG. 7. A log–log plot of Nusselt number vs Rayleigh number. The various b values correspond to different scaling laws of the form Nu ∝ Ra^b, and the cyan asterisk shows the result from the 3D simulation.

power laws do a reasonably good job in parts of Ra space.

The scaling exponents given in Fig. 7 are different from the canonical value of 1/3, and Nu is generally larger than what is found from the parameterization of Kelley (1990) in this range of Ra. A summary of different scalings found in the literature as well as the predictions from GL theory that we will discuss later in this section are found in Table 1. The fact that our exponents are different from 1/3 implies that F_T is not independent of H in our parameter range. An exponent smaller (larger) than 1/3 suggests F_T is a decaying (growing) function of H. Exponents smaller than 1/3 have been found before in the literature. Both Kelley (1990) and Flanagan et al. (2013) find exponents close to 0.28 [in the case of Flanagan et al. (2013), we have recalculated their exponent from the $H \in [1, 4]$ m simulations, which is presented as a $F_T \propto T^c$ law, using the fixed relationship between ΔT and H in their runs]. This is close to the exponent we find in our high Ra runs (Ra ∈ [1.6 × 10^7, 8.2 × 10^7]). As a complement to experimental estimates, Kelley (1990) also derived a simple model in which a Ra exponent smaller than 1/3 can be rationalized if a significant part of the kinetic energy dissipation occurs in the boundary layer. Later on in this section we shall see that this is, in fact, the case in our simulations.

Another interesting finding is the very small exponent found for Ra ∈ [1.5 × 10^6, 1.6 × 10^7]. We are not aware of such a small Ra exponent ever being found for double diffusion. Although it should be noted that a recalculation of the exponent from Flanagan et al. (2013) and also using their run with $H = 0.5$ m gives an exponent of 0.25. So it appears that a lower exponent is evident also in the lowest Ra run of Flanagan et al. (2013). This is also consistent with our runs since the smallest Ra in Flanagan et al. (2013) is 1.59 × 10^6, which is within the range where we find an exponent of about 0.09, while their second smallest Ra = 3 × 10^7 is within the 0.28 range also in our simulations. A small exponent (perhaps even a negative) for $R_\rho = 5$ and Ra of approximately 10^6–10^7 is also hinted at in Fig. 11a of Scheifele et al. (2014). Moreover, the four heat flux scaling runs in Flanagan et al. (2013) were all done in 3D and appear to show good consistency with our 2D runs where the Ra ranges overlap. Good consistency between 2D and 3D runs have also been found for thermal convection when Pr > 1 (Schmalzl et al. 2004). Whether this condition also applies to diffusive convection is, however, not known.

b. GL theory

GL theory has, as we briefly mentioned in the introduction, proven very successful in predicting heat

TABLE 1. Suggested heat flux scaling laws for diffusive convection. A single asterisk indicates that both the theoretical prediction and the laboratory experiments in Kelley (1990) are based on thermal convection. Two asterisks indicate that the difference in values is due to differences in how they define H used to compute Ra. Three versions were considered: H based on the mixed layer thickness above the interface, H based on the mixed layer thickness below the interface, and the average of the two. The first two versions both give 0.29, and the averaged version gives 0.25. The averaged version is also the one used by Sommer et al. (2013). Three asterisks indicate the 1/3 scaling does not occur in the Ra range of our simulation but is expected to occur for higher Ra. Four asterisks indicate this regime occupies a small parameter range and has never been observed cleanly for thermal convection. There is, however, evidence for it from the effect it has on neighboring regimes (D. Lohse 2016, personal communication).

Study	Ra exponent	Ra range	Method
Turner (1965)	1/3	N/A	Theory
Kelley (1990)	0.284*(0.27*)	10^4–10^{10} (10^7–10^{10})	Laboratory experiments (theory)
Flanagan et al. (2013)	0.28 (0.25)	$3 \times 10^7 - 7.6 \times 10^9$ ($1.9 \times 10^6 - 7.6 \times 10^9$)	DNS
Sommer et al. (2013)	1/5	10^5–10^{10}	Measurements
Guthrie et al. (2015)	0.29**(0.25**)	10^5–10^{11}	Measurements
The current study	0.27 (0.09)	$1.6 \times 10^7 - 8.2 \times 10^7$ ($1.5 \times 10^6 - 1.6 \times 10^7$)	DNS
GL theory	1/3***, 1/4, 1/5****	N/A	Theory

fluxes in turbulent Rayleigh–Bénard convection (Ahlers et al. 2009). Yang et al. (2015) applied the GL theory to the salt-finger case and found a good agreement with observations. Given that the diffusive case of double-diffusive convection is in many ways more similar to Rayleigh–Bénard convection than the salt-finger case is, it seems likely that GL theory might prove useful also for the diffusive regime. In what follows, we will examine this idea, but first we will briefly go through the theory for completeness. The basis for the GL theory is the following two equations:

$$\varepsilon_u = \frac{\mathrm{RaPr}^{-2}\nu^3}{H^4}(\mathrm{Nu}-1), \tag{28}$$

and

$$\varepsilon_T = \frac{\mathrm{Nu}\Delta T^2 \kappa_T}{H^2}. \tag{29}$$

These are exact relations in the Rayleigh–Bénard case due to the insulating boundary conditions. Rayleigh–Bénard convection is thus governed by the nondimensional numbers Ra and Pr and the system response is given by Nu and $\mathrm{Re} = UH/\nu$, where Re is the Reynolds number, and U is a velocity scale, characteristic of the circulation cell in the mixed layer. The first step in deriving the GL theory is to set $\varepsilon_u = \varepsilon_u^{\mathrm{ML}} + \varepsilon_u^{\mathrm{BL}}$ and $\varepsilon_T = \varepsilon_T^{\mathrm{ML}} + \varepsilon_T^{\mathrm{BL}}$, where the superscript ML indicates the mixed layer and the superscript BL indicates the boundary layer. The theory thus separates the dissipations into mixed layer and boundary layer contributions. To be able to solve (28) and (29) for Nu and Re, different estimates for $\varepsilon_u^{\mathrm{ML}}$, $\varepsilon_u^{\mathrm{BL}}$, $\varepsilon_T^{\mathrm{ML}}$, and $\varepsilon_T^{\mathrm{BL}}$ are introduced. The derivation of these estimates is quite lengthy, so the interested reader is referred to Grossmann and Lohse (2000) for details.

Four different regimes exist, assuming that the dissipations are completely bulk or boundary layer dominated. Another four subregimes exist to distinguish the cases depending on whether the thermal h_T or viscous h_ν boundary layer is thicker, since this difference changes the estimate of ε_T. The scaling laws for all eight completely mixed layer– or boundary layer–dominated regimes are found in Table 2.

Apart from these eight scaling regimes, the theory has also been extended to a model that can transition between these regimes in a continuous manner; Nu and Re are then given by these coupled nonlinear equations:

$$(\mathrm{Nu}-1)\mathrm{RaPr}^{-2} = c_1 \frac{\mathrm{Re}^2}{g(\sqrt{\mathrm{Re}_L}/\mathrm{Re})} + c_2 \mathrm{Re}^3, \tag{30}$$

and

$$\mathrm{Nu} - 1 = c_3 \mathrm{Re}^{1/2}\mathrm{Pr}^{1/2}\left\{ f\left[\frac{2a\mathrm{Nu}}{\sqrt{\mathrm{Re}_L}} g\left(\sqrt{\frac{\mathrm{Re}_L}{\mathrm{Re}}}\right)\right]\right\}^{1/2} + c_4 \mathrm{Pr}\,\mathrm{Re} f\left[\frac{2a\mathrm{Nu}}{\sqrt{\mathrm{Re}_L}} g\left(\sqrt{\frac{\mathrm{Re}_L}{\mathrm{Re}}}\right)\right], \tag{31}$$

where c_1, c_2, c_3, c_4, and a are tunable parameters, and $\mathrm{Re}_L = (2a)^2$ is a critical Reynolds number that has been

TABLE 2. Heat flux scaling laws for the different regimes in the GL theory.

	$\varepsilon_u \approx \varepsilon_u^{\mathrm{ML}}$, $\varepsilon_T \approx \varepsilon_T^{\mathrm{ML}}$	$\varepsilon_u \approx \varepsilon_u^{\mathrm{ML}}$, $\varepsilon_T \approx \varepsilon_T^{\mathrm{BL}}$	$\varepsilon_u \approx \varepsilon_u^{\mathrm{BL}}$, $\varepsilon_T \approx \varepsilon_T^{\mathrm{ML}}$	$\varepsilon_u \approx \varepsilon_u^{\mathrm{BL}}$, $\varepsilon_T \approx \varepsilon_T^{\mathrm{BL}}$
$h_\nu > h_T$	$\mathrm{Nu} \propto \mathrm{Ra}^{1/3}$	$\mathrm{Nu} \propto \mathrm{Ra}^{1/5}$	$\mathrm{Nu} \propto \mathrm{Ra}^{3/7}\mathrm{Pr}^{-1/7}$	$\mathrm{Nu} \propto \mathrm{Ra}^{1/4}\mathrm{Pr}^{-1/12}$
$h_\nu < h_T$	$\mathrm{Nu} \propto \mathrm{Ra}^{1/2}\mathrm{Pr}^{1/2}$	$\mathrm{Nu} \propto \mathrm{Ra}^{1/5}\mathrm{Pr}^{1/5}$	$\mathrm{Nu} \propto \mathrm{Ra}^{2/3}\mathrm{Pr}^{1/3}$	$\mathrm{Nu} \propto \mathrm{Ra}^{1/4}\mathrm{Pr}^{1/8}$

introduced together with the empirically determined functions $f(x) = (1 + x^4)^{1/4}$ and $g(x) = x(1 + x^4)^{1/4}$ to enable transitions between the different regimes. Values of the tuning parameters appropriate for Rayleigh–Bénard convection are given in Grossmann and Lohse (2001), and it is argued that these can be used also for double diffusion by Yang et al. (2015).

Equation (29) is equivalent to our (25), so no modifications are needed for the double-diffusive case. The appropriate form of (28) for double diffusion can be found from (16) and looks like

$$\varepsilon_u = \frac{\mathrm{Ra}\,\mathrm{Pr}^{-2}\nu^3}{H^4}[\mathrm{Nu}(1 - R_f) - 1 + \tau R_\rho]. \qquad (32)$$

In our DNS, we have $\tau = 0.01$, $R_\rho = 5$, and $R_f \approx 0.14$. These values suggest that (32) is close to (28) and that perhaps GL theory can be applied unmodified to the double-diffusive case. Yang et al. (2015) applied the theory without modifications to the salt-finger case with a good result, and we shall start with that approach as well.

Using our DNS, we can diagnose how the dissipation is partitioned between the mixed and boundary layers. Figure 8 shows the kinetic energy dissipation as a function of z_T^* and z_S^*, where z_T^* is defined as

$$z_T^* = \left|2\frac{z - H}{h_T}\right|, \qquad (33)$$

and h_T, the thermal interface thickness, is given by $h_T = \kappa_T \Delta T/F_T$. The definition of z_S^* is analogous but uses h_S instead of h_T. We thus have $z_T^* = 1$ ($z_S^* = 1$) at the edge of the thermal (haline) boundary layer. Slightly less than 30% of the kinetic energy dissipation typically occurs within the thermal boundary layer in our runs. We thus know that ε_u has important contributions both from the boundary and mixed layer, given that $h_\nu \geq h_T$. Figure 9 shows that ε_T is mostly boundary layer dominated. To derive the heat flux scaling from GL theory we must also determine the relative size of the thermal and viscous boundary layers. The thermal and haline boundary layer thicknesses (h_T and h_S) are easy to estimate, while the viscous boundary layer thickness is more difficult. Petschel et al. (2013) sought to remedy this problem by introducing so-called dissipation layers. Dissipation is typically enhanced in the boundary layers, and the edge of a dissipation layer is defined as the distance from the boundary where the horizontally averaged dissipation equals the volume average. This definition can be used just as easily on thermal or haline variance dissipation as on kinetic energy dissipation. However, the kinetic energy dissipation in the center of the interfaces is often weaker than the volume-averaged dissipation in our runs. When this is the case, one gets a nonexistent dissipation layer with the definition above. To remedy this problem we define the dissipation layer as the distance from the boundary to the level outside of the dissipation peak where the horizontally averaged dissipation equals the volume average.

Figure 10 shows how the thermal and haline dissipation layer thicknesses (h_{ε_T} and h_{ε_S}) compare to the usual boundary layer thicknesses h_T and h_S. For the viscous boundary layer thickness (we call it h_{ε_u} rather than h_ν here to signify that it is a dissipation layer), we get two different estimates depending on whether the zero isohaline or isotherm is chosen to be the boundary (these are distinguished by having S or T as a superscript). The dissipation layer definition is more robust for tracer variance than for kinetic energy dissipation, where we see a larger spread in the estimates. All our runs have $h_\nu > h_T$. The kinetic energy dissipation thus appears to have an important contribution both from the mixed layer and the boundary layer, while the thermal variance dissipation is mostly boundary layer dominated (see Figs. 8 and 9). For $\varepsilon_T \approx \varepsilon_T^{\mathrm{BL}}$, GL theory gives $\mathrm{Nu} \propto \mathrm{Ra}^{1/5}$, when ε_u is mixed layer dominated and $\mathrm{Nu} \propto \mathrm{Ra}^{1/4}\mathrm{Pr}^{-1/12}$ for the boundary layer–dominated regime. However, the 1/5 regime has never been observed cleanly in any laboratory or numerical experiments for thermal convection, only its effect on neighboring regimes has been observed (D. Lohse 2016, personal communication). Indeed, Grossmann and Lohse (2000) suggest that a vast majority of all reported convection experiments are within or close to the 1/4 regime and that the often reported exponents close to 0.28 are due to the influence of the neighboring 1/3 regime that occurs for higher Ra. This is a reasonable explanation also for our findings and those of Flanagan et al. (2013). Moreover, it should also be noted that if we use only the two runs with the highest Ra to calculate an exponent, we get 0.288, instead of 0.267, so there is a tendency toward larger exponents for higher Ra both in our simulations and in those of Flanagan et al. (2013), which is consistent with a gradual transition from a 1/4 to a 1/3 exponent.

To make a more exact extension of the GL theory to double diffusion, we must include also the salinity variance equation. Figure 9 shows that the haline boundary layer is thinner than the thermal and thus also the kinetic. The suggested scaling in the thermal case is

$$\mathrm{Nu} \propto \mathrm{Re}^{1/2}\mathrm{Pr}^{1/2}, \qquad (34)$$

when $h_T > h_\nu$, and

$$\mathrm{Nu} \propto \mathrm{Re}^{1/2}\mathrm{Pr}^{1/3}, \qquad (35)$$

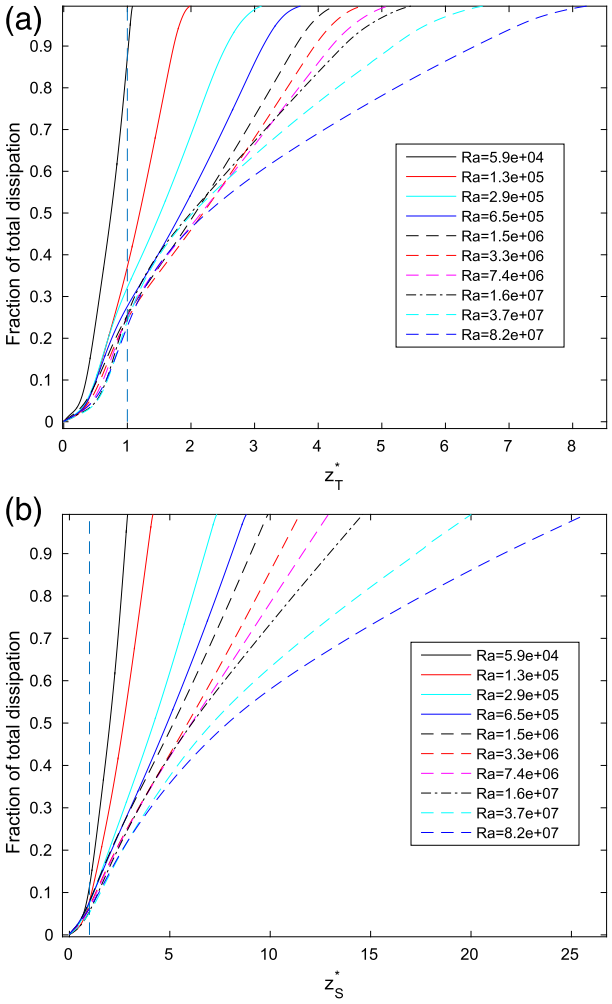

FIG. 8. Kinetic energy dissipation as a function of (a) z_T^* and (b) z_S^*. The total dissipation is normalized so that it is 1 in all cases. Values shown are cumulative, that is, they show the amount of dissipation that occurs between $z_T^* = 0$ ($z_S^* = 0$) and the coordinate value on the x axis. The vertical lines are situated at $z_T^* = 1$ and $z_S^* = 1$ and signify the edges of the boundary layer.

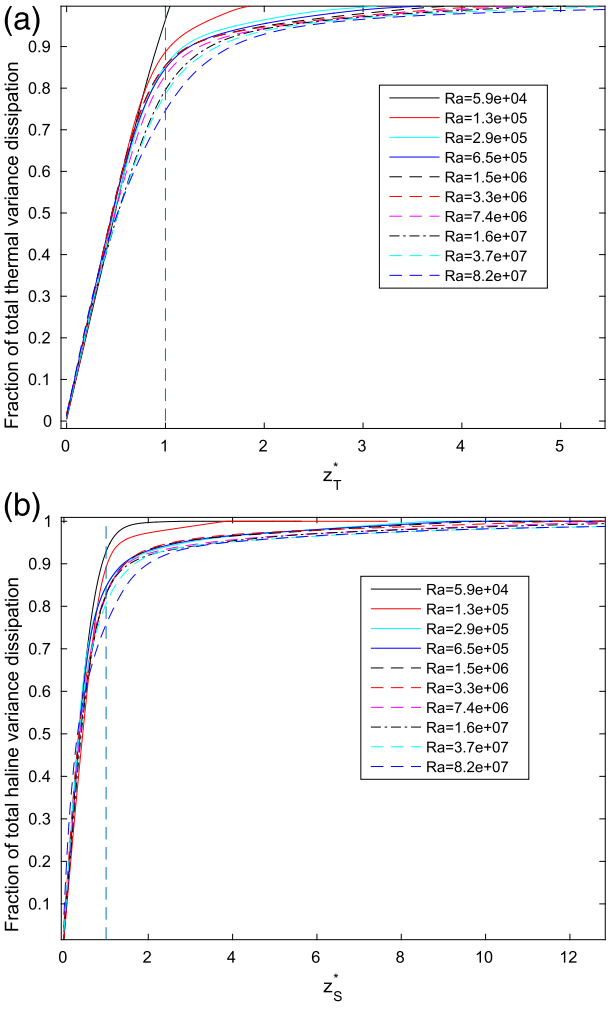

FIG. 9. As in Fig. 8, but for thermal and haline variance dissipation.

when $h_T < h_\nu$. How these scalings are derived is shown in appendix B. Using the same reasoning in the salinity case gives equations similar to (34) and (35), but where Nu is substituted for Nu_S (the Nusselt number for the salinity flux) and Pr is substituted for $\mathrm{Sc} = \nu/\kappa_S$ (the Schmidt number). Given that $h_S < h_\nu$, it is the latter approximation that is of interest to us. Now we can use the scaling laws (34) and (35) in the exact relation

$$\frac{\mathrm{Nu}_S}{\mathrm{Nu}} = \frac{R_f}{R_\rho \tau} \tag{36}$$

to get an expression for R_f, which can then be eliminated from (32). The most relevant case for us is $h_T < h_\nu$ and $h_S < h_\nu$, which gives $R_f \propto R_\rho \tau^{2/3}$. Another option is that $h_T > h_\nu$ and $h_S < h_\nu$, in which case we get $R_f \propto R_\rho \tau^{2/3} \mathrm{Pr}^{-1/6}$. One last option that is probably not so important in oceanography is that $h_T > h_\nu$ and $h_S > h_\nu$, which leads to $R_f \propto R_\rho \tau^{1/2}$.

Carpenter et al. (2012) show an extensive list of earlier estimates of R_f. The only exponent suggested for the R_ρ dependence, except zero, has been 1, which is proposed by Newell (1984), Fernando (1989), and Carpenter et al. (2012). For the τ dependence, there is a much larger spread in the estimates: Newell (1984) finds an exponent of 1, and an exponent of ½ is found by Shirtcliffe (1973), Linden and Shirtcliffe (1978), Fernando (1989), and Stamp et al. (1998), while Takao and Narusawa (1980) finds an exponent of −⅓. Carpenter et al. (2012), meanwhile, found an exponent of 4/5. The GL prediction of ⅔ is thus well within the range of earlier estimates. It is interesting that the most commonly found value of ½ is the one we arrived at

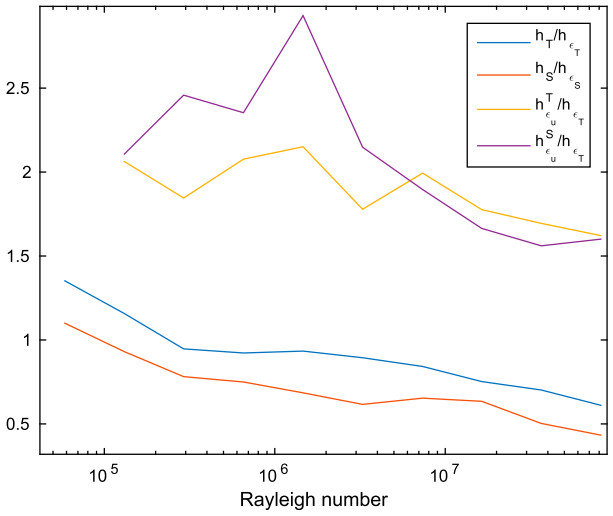

FIG. 10. Comparison of the boundary layer thickness based on the conventional definition and as dissipation layers (Petschel et al. 2013).

when $h_T > h_\nu$ and $h_S > h_\nu$, a situation that seems unlikely to occur in a heat–salt system.

6. Discussion and conclusions

The large Rayleigh numbers that often occur in diffusive staircases in the ocean are difficult to achieve both in numerical simulations and in laboratory experiments. This poses a difficult challenge for researchers trying to derive accurate flux laws. In this paper, we have focused on a range of Rayleigh numbers that commonly occur both in lakes (Sommer et al. 2013; Scheifele et al. 2014) and in the Amundsen Basin in the Arctic Ocean (Guthrie et al. 2015), as can be seen in our Fig. 5. This choice of focus is not done simply because of the earlier success the model has had in simulating the diffusive convection in Lake Kivu (Sommer et al. 2014). It is rather limitations in computational power that limits our ability to simulate higher Rayleigh number environments for long enough times to achieve a steady state. This is one of the reasons why GL theory may prove very useful in oceanography. For GL theory to be useful in the oceanographic context, it is enough to know how the tracer variance and the kinetic energy dissipation are partitioned between the mixed and the boundary layer. This type of information can potentially also be found from microstructure field measurements, which could greatly extend our knowledge of what scaling laws apply for double diffusion in the high Ra range that is currently beyond our modeling capabilities.

In any case, it has become quite clear through this and earlier work (e.g., Kelley 1990; Flanagan et al. 2013) that the 4/3 law is an over simplification and often inadequate to parameterize double-diffusive fluxes in the oceans. In fact, the 1/3 exponent on the Rayleigh number that is a necessity for the 4/3 law is not found in any our runs, and, to our knowledge, neither is it found in any other experimental study of diffusive convection (see Table 1). Furthermore, it is clear from our runs that the range of Rayleigh numbers in nature is too large to accommodate an accurate flux law with a single Ra exponent; the flux laws must therefore be functions of the Rayleigh number, just as in the GL theory for thermal convection. This does not mean, however, that the 1/3 exponent and its consequence, the 4/3 law, is always inaccurate. For thermal convection there is a regime with a 1/3 exponent that occurs when both kinetic energy and thermal variance is mixed layer dominated and $h_\nu > h_T$. This is likely to occur also for double diffusion at high enough Ra and may well be the case in some of the thicker diffusive layers in the Arctic Ocean. In fact, Guthrie et al. (2015) found a decent agreement between observed fluxes and fluxes calculated using the 1/3 exponent, although the agreement was even better with a 0.29 exponent. More research is needed before we can propose an accurate flux law for diffusive convection that applies to all ocean and lake environments. However, we think that the method of characterizing the flow by how the dissipation is partitioned between the boundary and the mixed layer used in the GL theory, and in this manuscript, is a step toward finding a universal flux law for diffusive convection. Such a flux law is a necessity for an accurate description of double-diffusive fluxes in future GCMs and is therefore of great importance for oceanography and climate studies.

With our current knowledge, it is at least possible to pinpoint some likely regimes that occur for different Ra. However, caution is needed since the Ra exponent may also be a function of R_ρ, and more experiments are needed to investigate such a functional dependence. In our experiments, which are to our knowledge the only experiments that probe also very low Ra, we found that a power law does not give an accurate description of the fluxes for Ra much lower than 10^6. We also find a small range in between $10^6 < \mathrm{Ra} < 10^7$, where a very low exponent of 0.09 is found. Whether this small range is better thought of as a regime of its own or as the upper part of the region where a power law is inaccurate is not clear. However, there is at least clear support from the simulations of Flanagan et al. (2013) that the exponent in this range is smaller than those typically found for diffusive convection at a higher Rayleigh number. An exponent of 0.28 is found by Flanagan et al. (2013) in the Rayleigh number range between 3×10^7 and 7.6×10^9. We find a similar exponent (0.27) for Ra between 1.6×10^7 and 8.2×10^7. The

question of if there exists an upper Ra limit for this scaling, as it does in thermal convection, is an important one that requires further experiments at higher Ra before it can be answered. Caution is therefore advised, since it is not possible to state whether the 0.27–0.29 scaling prevails throughout the higher end of the Ra distribution in oceanic staircases. The differences in the observationally estimated exponents of Sommer et al. (2013; 0.2) and Guthrie et al. (2015; 0.29), mentioned in the introduction, could perhaps then be explained by the fact that the average Ra is smaller in Lake Kivu than in the Amundsen Basin of the Arctic Ocean.

The next topic to discuss is how well the predictions from the GL theory agree with the results of our DNS experiments. As discussed before, an exponent close to 0.28 is often found also for thermal convection, and even though none of the regimes in the GL theory gives this scaling, it is rationalized as a superposition of the 1/4 and 1/3 regime. The 1/4 regime occurs when both thermal variance and kinetic energy is boundary layer dominated, while the 1/3 regime occurs when they are both mixed layer dominated. Our runs are clearly between these regimes and are thus in agreement with the theory. This is, however, not a very strong support of the theory's applicability to diffusive convection since the Ra range between the 1/4 and 1/3 regimes may be very large. Our DNS at high Ra appear to be close to a regime where the thermal variance dissipation is boundary layer dominated and the kinetic energy dissipation is mixed layer dominated. This regime has the scaling exponent 1/5 in the GL theory. This regime is absent in our simulations. This may, however, be explained by the fact that for thermal convection this regime occupies a small parameter range and has never been found cleanly in any laboratory or numerical experiments (D. Lohse 2016, personal communication). However, Sommer et al. (2013) found an exponent of 1/5 for their Lake Kivu data, so perhaps it is more prevalent for diffusive convection. One may summarize by saying that the findings from our DNS are in agreement with GL theory, but a much larger parameter range would have to be probed in order to really put the theory to the test.

Another important finding in this work is the excellent performance of the simplified energy and variance budgets. The three-term energy balance is especially of interest, since it corresponds to a slight modification of the integrated Osborn (1980) relation. This modification becomes less important as Ra increases but is still important in much of the relevant range for oceanography. Guthrie et al. (2015) shows that Ra $\in [10^6, 10^8]$ are commonly found in Arctic staircases, where we find that the volume-averaged diffusive buoyancy flux is about 20% of the interfacial buoyancy flux in this range, and thus that the volume-averaged advective buoyancy flux is significantly different from the interfacial buoyancy flux.

Acknowledgments. We thank Kraig Winters for the DNS code, Tobias Sommer and Alfred Wüest for providing the Lake Kivu data, and John Guthrie for providing the Arctic data. We also thank the two referees for their comments that have greatly improved the presentation of this work. Funding for this project was provided by the PACES II Programme of the Helmholtz Association.

APPENDIX A

Budgets with a Nonlinear Equation of State

In this section, we derive the energy budget for a diffusive staircase with a nonlinear equation of state under the Boussinesq approximation. The equations are the same as before, but we replace (5) with an expression for buoyancy of the form $b = \tilde{b}(S, T, z)$. The next step is to introduce the so-called Boussinesq dynamic enthalpy (Young 2010) defined as

$$\tilde{h}^{\ddagger}(S,T,z) \equiv \int_z^{z_{\mathrm{ref}}} \tilde{b}(S,T,z')\,dz', \tag{A1}$$

where z_{ref} is an arbitrarily chosen reference depth. The integral can be interpreted as the energy required to move a water parcel adiabatically from its vertical position z to the reference depth. The Boussinesq dynamic enthalpy plays the same role in the energy budget of the Boussinesq model with a nonlinear equation of state as the gravitational potential energy does in the Boussinesq model with a linear one. A budget equation for Boussinesq dynamic enthalpy is found by taking the material derivative of (A1) and integrating, which gives

$$\begin{aligned}\frac{d}{dt}\int_V \rho_0 h^{\ddagger}\,dV = &-\int_{\partial V} \rho_0 h^{\ddagger}\mathbf{u}_{\mathrm{out}}\cdot\hat{\mathbf{n}}\,dA + \int_V wg\rho'\,dV \\ &+\rho_0\int_{\partial V}\left(\kappa_T\nabla T\frac{\partial h^{\ddagger}}{\partial T}+\kappa_S\nabla S\frac{\partial h^{\ddagger}}{\partial S}\right)\cdot\hat{\mathbf{n}}\,dA - \rho_0\int_V\left(\kappa_T\nabla T\cdot\nabla\frac{\partial h^{\ddagger}}{\partial T}+\kappa_S\nabla S\cdot\nabla\frac{\partial h^{\ddagger}}{\partial S}\right)dV.\end{aligned} \tag{A2}$$

Using the same approximations as before and (14), we get a balance of the form

$$F_e = G_e + \varepsilon_u, \tag{A3}$$

where F_e is an interfacial dynamic enthalpy flux [the third term on the right-hand side of (A2)], and G_e is a generation term for dynamic enthalpy [the fourth term on the right-hand side of (A2)]. The difference between (20) and (A3) is thus that F_b is replaced by F_e and F_b^{cond} is replaced by G_e. The generation term can also be rewritten as

$$G_e = \int_V g\left(\kappa_T \frac{\partial \rho}{\partial T}\frac{\partial T}{\partial z} + \kappa_S \frac{\partial \rho}{\partial S}\frac{\partial S}{\partial z}\right) dV + \int_V \rho_0 \left[\kappa_T |\nabla T|^2 \frac{\partial^2 h^{\ddagger}}{\partial T^2} + \kappa_S |\nabla S|^2 \frac{\partial^2 h^{\ddagger}}{\partial S^2} + (\kappa_S + \kappa_T)\nabla S \cdot \nabla T \frac{\partial^2 h^{\ddagger}}{\partial S \partial T}\right] dV, \tag{A4}$$

which shows that the first term on the right-hand side of (A4) is equal to its sister term in the linear case [see(12)] but with the key difference that $(\partial\rho/\partial T)$ and $(\partial\rho/\partial S)$ are not assumed to be constants.

The numerical values of F_e and G_e depend on the choice of z_{ref}, since the partial derivatives of $h^{\ddagger}$ with respect to S and T grow with the distance $|z - z_{\text{ref}}|$. This means that if we choose z_{ref} to be far from z then F_e will grow and this growth will be balanced by a growth in the second term in G_e, while the first term in G_e will remain unchanged. Conversely, if we choose z_{ref} to be close to the depth of the mixed layer, then F_e and the second term in G_e will be small.

If we do as before and put $z = 0$ at the center of the top interface, $z = -H$ at center of the bottom interface, and $z_{\text{ref}} = 0$, we get the following expression for F_e:

$$F_e = g\int_{\partial V_b} \left(\kappa_T \nabla T \int_{-H}^{0} \frac{\partial \rho}{\partial T} dz + \kappa_S \nabla S \int_{-H}^{0} \frac{\partial \rho}{\partial S} dz\right) \cdot \hat{\mathbf{n}}\, dA, \tag{A5}$$

which, as we can see, reduces to F_b from the linear case if $(\partial\rho/\partial T)$ and $(\partial\rho/\partial S)$ are constants.

It is also instructive to look at the buoyancy budget with a nonlinear equation of state. Equation (8) of Hieronymus and Nycander (2013) gives this expression for the buoyancy sink due to the effects of the nonlinear equation of state:

$$\int_{\partial V} \frac{\partial b}{\partial T}\mathbf{F}_T \cdot \hat{\mathbf{n}}\, dA = \int_V Q\, dV, \tag{A6}$$

where Q is the buoyancy sink within the domain, and $(\partial b/\partial T)\mathbf{F}_T$ is the buoyancy flux due to the heat flux. The contribution from the salinity flux is negligible, since $(\partial b/\partial S)$ is nearly constant. The physical meaning of (A6) is that for a steady state to be possible, a net buoyancy flux into (out of) the domain must be compensated by a sink (source) within the domain. For a diffusive staircase, (A6) can be written as

$$\langle F_T \rangle_{xy} \frac{\Delta \frac{\partial b}{\partial T}}{H} = \langle Q \rangle_{xyz}, \tag{A7}$$

where $\Delta(\partial b/\partial T) = (\partial b/\partial T)(z = 0) - (\partial b/\partial T)(z = -H)$. The term $\langle Q \rangle_{xyz}$ is thus always negative in a diffusive staircase, since $(\partial b/\partial T)$ increases with both increased pressure and temperature. Buoyancy is therefore always consumed within diffusive staircases. The only thing that changes in the salt-finger case is that $\Delta(\partial b/\partial T) = (\partial b/\partial T)(z = -H) - (\partial b/\partial T)(z = 0)$. However, this change implies that $\langle Q \rangle_{xyz}$ may have either sign, since the increase in $(\partial b/\partial T)$ due to temperature can be balanced by that due to pressure.

The fact that the buoyancy flux is different at the top and bottom of an interface due to the difference in temperature was discovered more than 30 yr ago by McDougall (1981a,b). McDougall (1981b) also observed how this led to interface migration for strong temperature differences. It is therefore doubtful to what extent the zero interfacial advection assumption can be justified in the presence of nonlinear equation of state effects.

APPENDIX B

Deriving the Scaling Law for Boundary Layer–Dominated Salinity Variance Dissipation

Here, we look in more detail on how the GL theory scales $\varepsilon_T^{\text{BL}}$ and how we can use this to find a scaling for $\varepsilon_S^{\text{BL}}$. The most straightforward scaling for (29), or its salinity counterpart, in the boundary layer–dominated case is $\varepsilon_T^{\text{BL}} \propto \kappa_T \Delta T^2 \text{Nu} H^{-2}$; however, this information corresponds exactly to (29), so it is not useful. The path taken by Grossmann and Lohse (2000) is instead to use the heat equation in the thermal boundary layer. The equation is

$$u\frac{\partial T}{\partial x} + w\frac{\partial T}{\partial z} = \kappa_T \frac{\partial^2 T}{\partial T^2}. \tag{B1}$$

They then argue that the two terms on the left-hand side are of the same order and thus that $\partial_x \propto H^{-1}$ and $\kappa_T \partial_z^2 \propto \kappa_T h_T^{-2}$. The velocity scale U is used when $h_T > h_\nu$, and $U h_T h_\nu^{-1}$ is used when $h_T < h_\nu$. This leads to

$$\text{Nu} \propto \text{Re}^{1/2}\text{Pr}^{1/2} \tag{B2}$$

in the first case and

$$\mathrm{Nu} \propto \mathrm{Re}^{1/2}\mathrm{Pr}^{1/3} \tag{B3}$$

in the second. Here, we used H also as a horizontal length scale. In Rayleigh–Bénard convection where we have a square domain with solid walls, this is an obvious choice, but in double diffusion in nature, the horizontal length scale is typically many orders of magnitude larger than the vertical. However, the horizontal extent of individual convection cells is likely similar to the vertical one, which serves as our justification. Another option is to instead focus on the vertical advection term; this has the advantage that it is evident that the same temperature or salinity scale can be used. Using $w \propto Uh_T H^{-1}$ also gives the scalings (B2) and (B3). The scaling for w here is derived using continuity and assuming H is the relevant horizontal length scale.

REFERENCES

Ahlers, G., S. Grossmann, and D. Lohse, 2009: Heat transfer and large scale dynamics in turbulent Rayleigh-Bénard convection. *Rev. Mod. Phys.*, **81**, 503, doi:10.1103/RevModPhys.81.503.

Carpenter, J. R., and M.-L. Timmermans, 2014: Does rotation influence double-diffusive fluxes in polar oceans? *J. Phys. Oceanogr.*, **44**, 289–296, doi:10.1175/JPO-D-13-098.1.

——, T. Sommer, and A. Wüest, 2012: Simulations of a double-diffusive interface in the diffusive convection regime. *J. Fluid Mech.*, **711**, 411–436, doi:10.1017/jfm.2012.399.

Farmer, D. M., and H. J. Freeland, 1983: The physical oceanography of fjords. *Prog. Oceanogr.*, **12**, 147–220, doi:10.1016/0079-6611(83)90004-6.

Fernando, H. J. S., 1989: Buoyancy transfer across a diffusive interface. *J. Fluid Mech.*, **209**, 1–34, doi:10.1017/S0022112089003010.

Flanagan, J. D., A. S. Lefler, and T. Radko, 2013: Heat transport through diffusive interfaces. *Geophys. Res. Lett.*, **40**, 2466–2470, doi:10.1002/grl.50440.

Foster, T. D., and E. C. Carmack, 1976: Temperature and salinity structure in the Weddell Sea. *J. Phys. Oceanogr.*, **6**, 36–44, doi:10.1175/1520-0485(1976)006<0036:TASSIT>2.0.CO;2.

Grossmann, S., and D. Lohse, 2000: Scaling in thermal convection: A unifying theory. *J. Fluid Mech.*, **407**, 27–56, doi:10.1017/S0022112099007545.

——, and ——, 2001: Thermal convection for large Prandtl numbers. *Phys. Rev. Lett.*, **86**, 3316–3319, doi:10.1103/PhysRevLett.86.3316.

——, and ——, 2002: Prandtl and Rayleigh number dependence of the Reynolds number in turbulent thermal convection. *Phys. Rev.*, **66**, 016305, doi:10.1103/PhysRevE.66.016305.

——, and ——, 2004: Fluctuations in turbulent Rayleigh-Bénard convection: The role of plumes. *Phys. Fluids*, **16**, 4462–4472, doi:10.1063/1.1807751.

Guthrie, J. D., I. Fer, and J. Morrison, 2015: Observational validation of the diffusive convection flux laws in the Amundsen Basin, Arctic Ocean. *J. Geophys. Res. Oceans*, **120**, 7880–7896, doi:10.1002/2015JC010884.

Hieronymus, M., and J. Nycander, 2013: The buoyancy budget with a nonlinear equation of state. *J. Phys. Oceanogr.*, **43**, 176–186, doi:10.1175/JPO-D-12-063.1.

——, and ——, 2015: Finding the minimum potential energy state by adiabatic parcel rearrangements with a nonlinear equation of state: An exact solution in polynomial time. *J. Phys. Oceanogr.*, **45**, 1843–1857, doi:10.1175/JPO-D-14-0174.1.

——, J. Nilsson, and J. Nycander, 2014: Water mass transformation in salinity–temperature space. *J. Phys. Oceanogr.*, **44**, 2547–2568, doi:10.1175/JPO-D-13-0257.1.

Kelley, D. E., 1990: Fluxes through diffusive staircases: A new formulation. *J. Geophys. Res.*, **95**, 3365–3371, doi:10.1029/JC095iC03p03365.

——, H. Fernando, A. Gargett, J. Tanny, and E. Özsoy, 2003: The diffusive regime of double-diffusive convection. *Prog. Oceanogr.*, **56**, 461–481, doi:10.1016/S0079-6611(03)00026-0.

Linden, P., and T. G. L. Shirtcliffe, 1978: The diffusive interface in double-diffusive convection. *J. Fluid Mech.*, **87**, 417–432, doi:10.1017/S002211207800169X.

McDougall, T. J., 1981a: Double-diffusive convection with a nonlinear equation of state: Part I. The accurate conservation of properties in a two-layer system. *Prog. Oceanogr.*, **10**, 71–89, doi:10.1016/0079-6611(81)90001-X.

——, 1981b: Double-diffusive convection with a nonlinear equation of state: Part II. Laboratory experiments and their interpretation. *Prog. Oceanogr.*, **10**, 91–121, doi:10.1016/0079-6611(81)90002-1.

——, and B. R. Ruddick, 1992: The use of ocean microstructure to quantify both turbulent mixing and salt-fingering. *Deep-Sea Res.*, **39A**, 1931–1952, doi:10.1016/0198-0149(92)90006-F.

Moin, P., and K. Mahesh, 1998: Direct numerical simulation: A tool in turbulence research. *Annu. Rev. Fluid Mech.*, **30**, 539–578, doi:10.1146/annurev.fluid.30.1.539.

Newell, T. A., 1984: Characteristics of a double-diffusive interface at high density stability ratios. *J. Fluid Mech.*, **149**, 385–401, doi:10.1017/S0022112084002718.

Nycander, J., 2011: Energy conversion, mixing energy, and neutral surfaces with a nonlinear equation of state. *J. Phys. Oceanogr.*, **41**, 28–41, doi:10.1175/2010JPO4250.1.

——, J. Nilsson, K. Döös, and G. Broström, 2007: Thermodynamic analysis of ocean circulation. *J. Phys. Oceanogr.*, **37**, 2038–2052, doi:10.1175/JPO3113.1.

Osborn, T. R., 1980: Estimates of the local rate of vertical diffusion from dissipation measurements. *J. Phys. Oceanogr.*, **10**, 83–89, doi:10.1175/1520-0485(1980)010<0083:EOTLRO>2.0.CO;2.

——, and C. S. Cox, 1972: Oceanic fine structure. *Geophys. Fluid Dyn.*, **3**, 321–345, doi:10.1080/03091927208236085.

Padman, L., and T. M. Dillon, 1989: Thermal microstructure and internal waves in the Canada Basin diffusive staircase. *Deep-Sea Res.*, **36A**, 531–542, doi:10.1016/0198-0149(89)90004-6.

Pérez-Santos, I., J. Garcés-Vargas, W. Schneider, L. Ross, S. Parra, and A. Valle-Levinson, 2014: Double-diffusive layering and mixing in Patagonian fjords. *Prog. Oceanogr.*, **129**, 35–49, doi:10.1016/j.pocean.2014.03.012.

Petschel, K., S. Stellmach, M. Wilczek, J. Lölff, and U. Hansen, 2013: Dissipation layers in Rayleigh-Bénard convection: A unifying view. *Phys. Rev. Lett.*, **110**, 114502, doi:10.1103/PhysRevLett.110.114502.

Radko, T., 2013: Double-Diffusive Convection. Cambridge University Press, 342 pp.

Scheifele, B., R. Pawlowicz, T. Sommer, and A. Wüest, 2014: Double diffusion in saline Powell Lake, British Columbia. *J. Phys. Oceanogr.*, **44**, 2893–2908, doi:10.1175/JPO-D-14-0070.1.

Schmalzl, J., M. Breuer, and U. Hansen, 2004: On the validity of two-dimensional numerical approaches to time-dependent

thermal convection. *Europhys. Lett.*, **67**, 390–396, doi:10.1209/epl/i2003-10298-4.

Shirtcliffe, T. G. L., 1973: Transport and profile measurements of the diffusive interface in double-diffusive convection with similar diffusivities. *J. Fluid Mech.*, **57**, 27–43, doi:10.1017/S002211207300100X.

Smyth, W. D., and J. Moum, 2000: Length scales of turbulence in stably stratified mixing layers. *Phys. Fluids*, **12**, 1327–1342, doi:10.1063/1.870385.

Sommer, T., J. R. Carpenter, M. Schmid, R. G. Lueck, M. Schurter, and A. Wüest, 2013: Interface structure and flux laws in a natural double-diffusive layering. *J. Geophys. Res. Oceans*, **118**, 6092–6106, doi:10.1002/2013JC009166.

——, ——, and A. Wüest, 2014: Double-diffusive interfaces in Lake Kivu reproduced by direct numerical simulations. *Geophys. Res. Lett.*, **41**, 5114–5121, doi:10.1002/2014GL060716.

Stamp, A. P., G. O. Hughes, R. I. Nokes, and R. W. Griffiths, 1998: The coupling of waves and convection. *J. Fluid Mech.*, **372**, 231–271, doi:10.1017/S0022112098002304.

Takao, S., and U. Narusawa, 1980: An experimental study of heat and mass transfer across a diffusive interface. *Int. J. Heat Mass Transfer*, **23**, 1283–1285, doi:10.1016/0017-9310(80)90058-7.

Timmermans, M.-L., J. Toole, R. Krishfield, and P. Winsor, 2008: Ice-tethered profiler observations of the double-diffusive staircase in the Canada Basin thermocline. *J. Geophys. Res.*, **113**, C00A02, doi:10.1029/2008JC004829.

Turner, J. S., 1965: The coupled turbulent transport of salt and heat across a sharp density interface. *Int. J. Heat Mass Transfer*, **8**, 759–767, doi:10.1016/0017-9310(65)90022-0.

——, 2010: The melting of ice in the Arctic Ocean: The influence of double-diffusive transport of heat from below. *J. Phys. Oceanogr.*, **40**, 249–256, doi:10.1175/2009JPO4279.1.

Winters, K. B., J. A. MacKinnon, and B. Mills, 2004: A spectral model for process studies of rotating, density-stratified flows. *J. Atmos. Oceanic Technol.*, **21**, 69–94, doi:10.1175/1520-0426(2004)021<0069:ASMFPS>2.0.CO;2.

Wüest, A., T. Sommer, M. Schmid, and J. R. Carpenter, 2012: Diffusive-type of double diffusion in lakes: A review. *Environmental Fluid Mechanics: Memorial Volume in Honor of Prof. Gerhard H. Jirka*, W. Rodi and M. Uhlmann, Eds., CRC Press, 271–284.

Yang, Y., E. P. van der Poel, R. Ostilla-Mónico, C. Sun, R. Verzicco, S. Grossmann, and D. Lohse, 2015: Salinity transfer in bounded double diffusive convection. *J. Fluid Mech.*, **768**, 476–491, doi:10.1017/jfm.2015.93.

Young, W. R., 2010: Dynamic enthalpy, conservative temperature, and the seawater Boussinesq approximation. *J. Phys. Oceanogr.*, **40**, 394–400, doi:10.1175/2009JPO4294.1.